Combined Wireless Power Transfer and Motor Driver System with a Single Converter

Enes Ayaz, Ogün Altun, Hakan Polat, Furkan Karakaya, Ozan Keysan

***Abstract*—In this paper, it is proposed that the existing converter used to drive the motor can also be utilized to excite the Wireless power transfer (WPT) coil instead of using an extra high-frequency converter. When the motor draws a low-frequency modulated current, the WPT system draws the high-frequency current harmonics of the switching frequency. Thus, a single converter is enough to simultaneous drive both the motor and the WPT system. Eliminating extra high-frequency converters brings some advantages resulting in that the system's complexity and cost are reduced. Besides, the development of wide-bandgap (WBG) devices such as GaN and SiC enables the operation of the motor driver converters at high switching frequencies with lower switching losses. Hence, the size of the WPT coils, which are excited by the motor driver, becomes reasonable. The proposed system has been tested experimentally using a GaN-based full-bridge converter. A series-series WPT at 50 W, and a DC motor at 500 W, have been operated simultaneously using the converter.**

***Index Terms*—Inductive Power Transfer(IPT), motor drivers, Wireless Power Transfer(WPT), slip rings,rotating systems**

I. Introduction

Power transfer to rotating systems is necessary for many applications such as electrical excited synchronous machines [1], solar wings [2], radar systems [3], wind turbines, etc. Slip rings can be used, which consist of copper rings and carbon brushes in contact with these rings, as shown in Fig. 1.a. However, slip rings are not reliable and require periodic maintenance since mechanical friction causes wear. Wireless power transfer (WPT) systems can be an alternative to slip rings [3], [4], thanks to increased reliability. The most common WPT topology used in slip ring applications is inductive power transfer (IPT), as shown in Fig. 1.b. The systems provide a flexible range of transfer distance and power ratings with higher efficiencies [5]. In IPT systems, the power is transferred by the magnetic coupling between the transmitter (Tx) and the receiver (Rx) coils, which are loosely coupled with inherently low power factors. Thus, compensation circuits are generally used, such as two-element (series-series (SS), series-parallel (SP), parallel-parallel (PP), parallel-series (PS)) [6], or hybrid compensation methods (LLC, LCC) [7], [8]. The Tx coil is excited with high-frequency AC, so a full-bridge converter (or single-phase inverter) is used. This extra converter increases the complexity and cost, thus reducing the feasibility of such systems. In this paper, a novel method that combines wireless power transfer and motor driver system with a single converter is proposed to overcome the problems of conventional slip rings and IPT systems with separate converters. The motor driver, shown in Fig. 1.b, already generates high-frequency switching harmonics, but the motor winding filters out these high-frequency components. In the proposed system, the Tx coil can be used to utilize these high-frequency voltage harmonics to transfer power to the Rx coil. Therefore, a separate IPT converter is no longer required, and the motor driver is also used as the IPT converter, which reduces the system's complexity, and cost of the overall systems, as illustrated in Fig. 1.c.

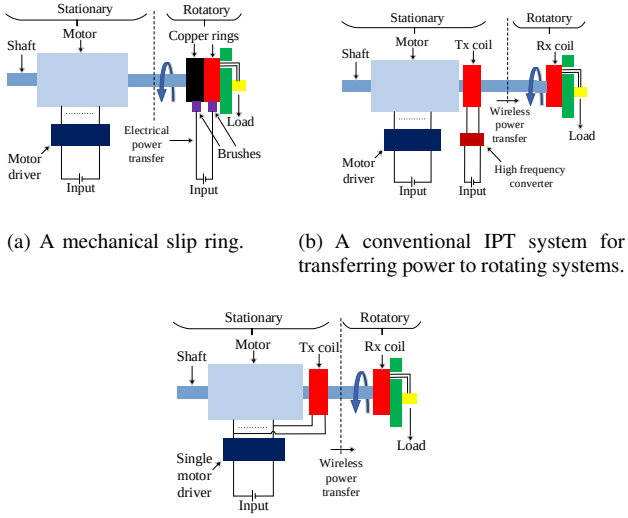

(a) A mechanical slip ring.

(b) A conventional IPT system for transferring power to rotating systems.

(c) The proposed IPT system for transferring power to rotating systems.

Fig. 1. Various systems transferring power to rotating systems.

A motor driver generates two distinctive harmonics at the switching frequency and the fundamental frequency. For conventional industrial motor drives, the switching frequency is usually below 20 kHz due to the switching losses of silicon (Si)-based devices [9]. In this frequency range, the IPT systems are not feasible as they get bulkier at lower frequencies [10]. However, recent developments in semiconductor technology pave the way for an increase in switching frequencies, with Silicon Carbide (SiC) or Gallium Nitride (GaN) based motor drivers [11], [12]. Besides their main advantages like lower conduction losses, small volume, and better cooling performance, wide band-gap (WBG) devices are capable of working at high switching frequencies [13]. Therefore, it is now possible to increase the switching frequency so that

Enes Ayaz, Ogün Altun, Hakan Polat, Furkan Karakaya,Ozan Keysan are with Middle East Technical University Power Lab, Department of Electrical and Electronics Engineering, Ankara, Turkey. Email: keysan@metu.edu.tr
Corresponding Author: Ozan Keysan, keysan@metu.edu.tr

practical IPT systems can be connected in parallel to the motor windings. The block diagram of the proposed system is shown in Fig. 2. Table I presents the advantages and disadvantages of the proposed system over conventional systems.

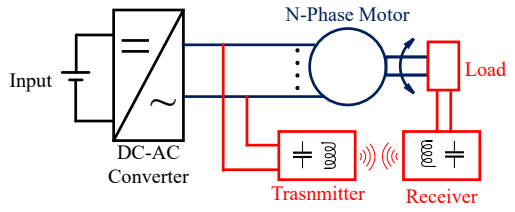

Fig. 2. The block diagram of the proposed IPT-based system with single converter.

TABLE I
COMPARISON OF VARIOUS SYSTEMS TRANSFERRING POWER TO ROTATING SYSTEMS

	Mechanical Slip Rings	Conventional IPT Systems	The Proposed IPT System
Reliability	- [14]	+ [3]	+
Maintenance	- [15]	+	+
Simplicity	+	-	+
Cost Effective	+	-	+
Efficiency	+	-	-

The proposed system meets the requirements and solves the complexity and cost problem of the conventional systems that use two converters: one for the motor driver and one for IPT. In conventional IPT systems, converters operate at zero voltage switching (ZVS) to reduce the switching losses [16]. Although the ZVS condition cannot be met in a single converter system due to motor currents, the switching loss of IPT is only a small fraction of the overall loss as power transfer to rotating systems are generally used to energize auxiliary systems, such as cameras, radar, sensors, and etc.

In this paper, a DC motor and an SS-IPT share a common GaN-based Full-Bridge (FB) converter. A 50 W IPT prototype will be tested while the motor driver runs the DC motor at 500 W.

II. System Proposal

In the proposed system, the motor and IPT systems are connected to a single FB converter, as shown in Fig. 3. The converter can be used for both driving the motor and transmitting wireless power if the following conditions are satisfied:

1) Output voltage of the converter should be not affected by the motor and IPT currents.
2) The motor and the IPT should have the same switching function.
3) There should be no circulation current between the motor winding and the IPT coil.

A. Output voltage of the converter

It is required that the motor and IPT currents do not affect the output voltage (V_o) of the converter. The converter generates a pulsating V_o that is not affected by the load currents

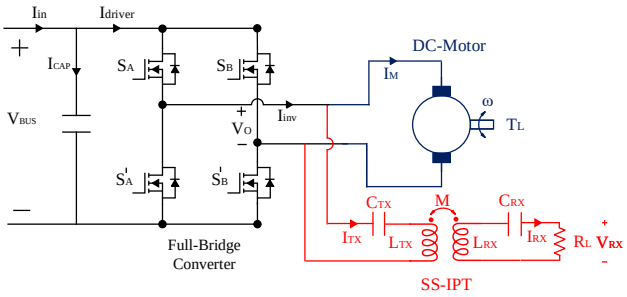

Fig. 3. Circuit diagram of the motor driver and the proposed IPT system with a single converter.

if the parasitic line or DC-link inductances are negligible. However, in a practical case, there will be a voltage drop in the DC-link due to high-frequency current components of the IPT side. This adverse effect can be reduced by minimizing parasitic inductances with proper layout design and using appropriate DC-link capacitance [17].

B. The switching pattern

A single converter can be implemented if the modulation method of the motor and IPT are the same. The challenge is to control the motor output power and IPT power independently using the same PWM waveforms. The converter controls the speed and torque of the DC motor by adjusting the DC output voltage. To obtain the desired voltage, a switching function of switching frequency (f_s) and duty cycle (D) is used, as presented in (1). Although the output voltage has switching harmonics, shown in Fig. 4, these harmonics are filtered by the motor's inductance.

$$S(t) = \mathrm{D} + \sum_{\mathrm{k}=1}^{\infty} \frac{2}{\mathrm{k}\pi} \sin(\mathrm{k}\pi\mathrm{D})\cos(2\pi\mathrm{k}\mathrm{f_s}\mathrm{t}) \qquad (1)$$

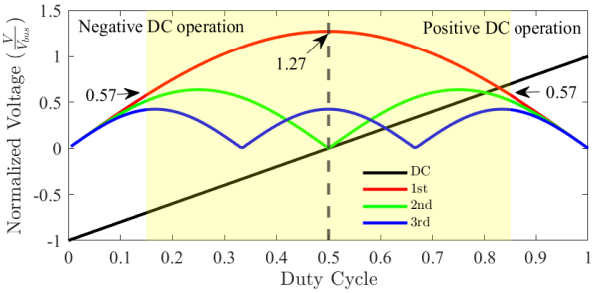

Fig. 4. The harmonic distribution of the converter's output voltage, which are obtained by analytically employing the switching function in the FB converter.

In a typical SS-IPT system, symmetrical PWM [18], having the same switching function as in (1) with a constant 0.5 duty cycle with variable frequency, can be employed. The IPT and motor cannot be combined in a single converter using the symmetrical PWM ($D = 0.5$), which does not provide DC output voltage. However, asymmetrical PWM [19], having the same switching function in (1) with a variable duty cycle and

frequency can be applied. Unlike the symmetrical PWM, the DC output voltage is controlled by the duty cycle. Hence, a combined converter can be achieved using asymmetrical PWM, which can control both the motor and the IPT system.

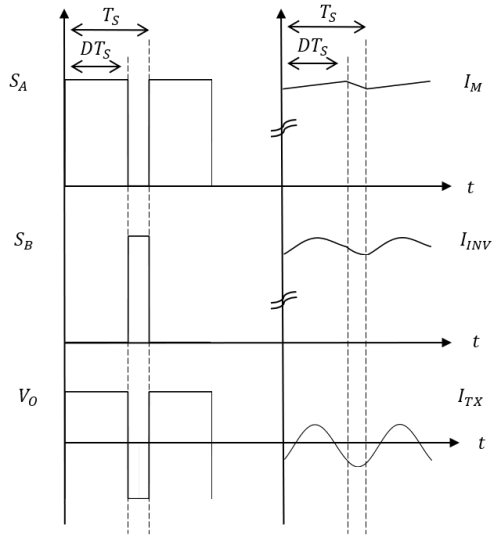

Fig. 5. Key waveforms of combined motor IPT systems

The fundamental waveforms of asymmetrical PWM are represented in Fig. 5 for the combined motor and IPT system. The gate signals of top switches of each leg (S_A and S_B, shown in Fig. 3) are given, and the switching pattern generates a pulsating output voltage (V_o), having DC and switching components. Besides, the motor current (I_M) is DC with small switching harmonics filtered out by motor windings. The Tx current (I_{TX}) is almost purely sinusoidal if the IPT has high quality. The inverter current (I_{INV}) is the sum of I_M and I_{TX}. However, the dominant current of the I_{INV} is the I_M since the IPT system is used for auxiliary systems, which have smaller power ratings than the motor.

C. Circulation currents between the motor and the IPT

Although the switching frequency of the motor and the IPT are the same, the operation frequencies of the motor and IPT are far away. The motor acts as a low pass filter, having a high impedance at the switching harmonics. The IPT operates at the switching frequency, and it acts as a band-pass filter, having a low impedance only near the resonant frequency of the IPT. Since their impedances are not matched, there will be no circulation current between the IPT coil and the motor windings, as will be discussed in the section IV.

III. System Design

In this section, the design procedure is presented for the proposed IPT system, the parameters of which are given in Table II. The input voltage is 100 V, and the motor is operated at a power of 500 W while IPT power is 50 W with 20 V Rx voltage.

TABLE II
The System Input-Output Specifications and The Parameters of The Motor and The Driver.

The Rated Voltages and Powers	
Input Voltage (V_{BUS})	100 V_{DC}
IPT Output Voltage (V_{RX})	20 V_{RMS}
Motor Output Power (P_M)	500W
IPT Output Power (P_O)	50W
The Motor Parameters	
Armature resistance (R_a)	2 Ω
Armature inductance (L_a)	7 mH
Motor electrical time constant (T_s)	3.5ms
The Driver Parameters	
Duty cycle(D)	$0.15 - 0.85$
Switching frequency (f_s)	$1 - 100$ kHz
Switching period (T_s)	$1\text{ms} - 10\mu\text{s}$

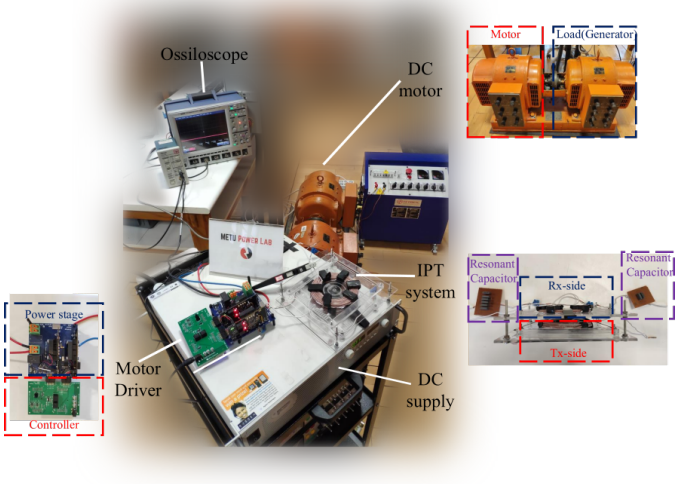

Fig. 6. The illustration of experimental setup.

A. Motor Driver

The motor and the driver setup include a separately excited DC machine and a GaN-based FB converter, as shown in Fig. 6. The FB converter consists of two GaN-based half-bridge boards as details described in [20]. The motor and the driver parameters are given in Table II. Although the converter is capable of working up to 450 kHz, there are some considerations to select the switching frequency. On the one hand, increasing switching frequency raises the driver's switching losses, reduces the driver's lifetime, and causes EMI problems. On the other hand, decreasing switching frequency increases the current and the torque ripples, depending on the motor's electrical time constant. The minimum switching frequency is 1 kHz because the motor has a higher electrical time constant as given in Table II. Besides, the maximum switching frequency is selected as 100 kHz by considering the switching losses of the driver.

B. IPT Design

In this paper, an SS-IPT topology is preferred as it provides an independent operation of the resonant frequency from load

conditions and mutual coupling. Since the IPT coils and the motor share the same converter, this independency provides flexibility at the design stage. After the topology is chosen, the resonant frequency should be properly defined as increasing the frequency shrinks the passive components but increases the coil losses. The resonant frequency is selected to operate between 65 kHz and 100 kHz, the upper limit of the motor driver. In addition, the distribution of switching harmonics is also varying with the duty cycle. The first harmonic of the switching, used in the IPT, becomes between $40\mathrm{V_{RMS}}$ and $90\mathrm{V_{RMS}}$ for 100 V DC-link and the duty cycle varies between 0.15 and 0.85. A systematical design for SS-IPT, implemented from [21], is applied. Firstly, the load resistance is found by using (2). Then, the Rx inductance can be calculated by using (3). The quality factor (Q_{RX}) should be between 1-10 as a rule of thumb. The Q_{RX} increases the size of the Rx coil but decreases the size of the Tx coil. Moreover, the mutual inductance can be calculated by using (4). The variation of the switching harmonics of the V_o affects the design of the IPT. The IPT is designed for the minimum voltage of the V_o since the power can be decreased by frequency control for higher voltage of the V_o.

$$\mathrm{R_L} = \frac{\mathrm{V_{RX}^2}}{\mathrm{P_o}} \tag{2}$$

$$\mathrm{L_{RX}} = \frac{\mathrm{Q_{RX}R_L}}{\omega_\mathrm{o}} \tag{3}$$

$$\mathrm{M} = \frac{\mathrm{V_o V_i}}{\mathrm{P_o}\omega_\mathrm{o}} \tag{4}$$

The value of the Tx coil can be found using (5). The coupling coefficient (k) varies between 0 and 1. Finally, the capacitance values can be achieved using (6).

$$\mathrm{L_{TX}} = \frac{\mathrm{V_i^2}}{\mathrm{k^2}\omega_\mathrm{o}^2\mathrm{Q_{RX}}} \tag{5}$$

$$\mathrm{C_{TX-RX}} = \frac{1}{\mathrm{L_{TX-RX}}}\mathrm{w_o^2} \tag{6}$$

The selection of k and Q_{RX} changes the IPT gain characteristic. In regular IPT systems, k is limited to keep the system bifurcation-free, which guarantees ZVS above the resonant frequency. However, in the proposed system, ZVS is not achieved due to the current of the motor. Hence, bifurcation-free design is not aimed in the system, and k should be selected regarding the Tx coil size. The change in the Tx inductances as a function of k is shown in Fig. 7.a. Increasing k decreases the size of the Tx coil. Besides, the variation on Tx and Rx inductances as a function of Q_{RX} is shown in Fig. 7.b. Q_{RX} increases the Rx coil, and the Tx coil decreases for a constant k. However, Q_{RX} and k affect the gain-frequency characteristics, shown in Fig. 7.c. Increasing both Q_{RX} and k leads the gain increase at frequencies below and above the resonant frequency. In this paper, Tx and Rx coil are desired to be in the 10-1000μH range, and the maximum gain is 0.5. Therefore, the Q_{RX} and k are selected as 0.40 and 2.6, respectively. In Table III, the finalized IPT system parameters are presented.

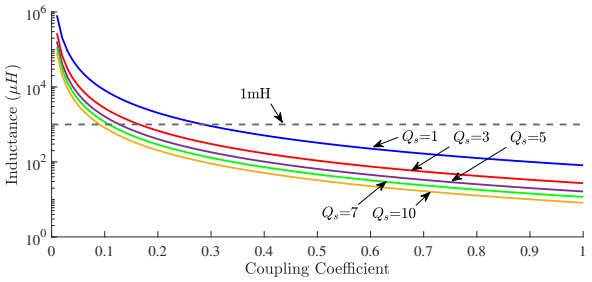

(a) The inductance of the Tx coil as a function of k.

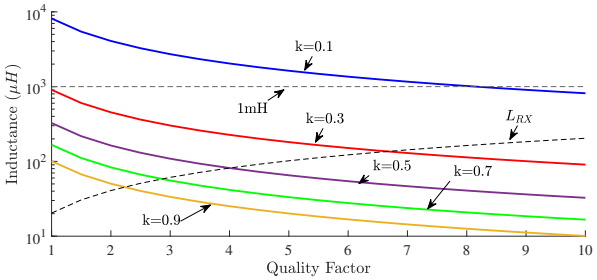

(b) The inductance of the Tx coil as a function of Qrx.

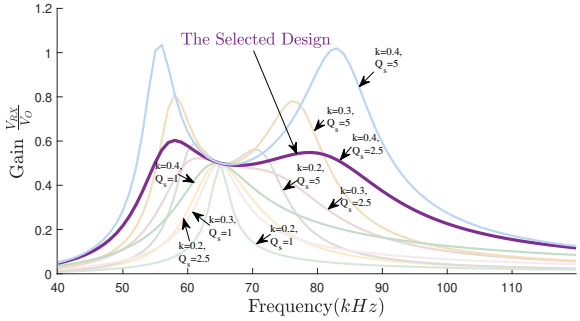

(c) The gain-frequency characteristic of several k and Qrx.

Fig. 7. Effect of the design parameters on Tx coil, Rx coil and gain of the IPT.

TABLE III
PARAMETERS OF THE IPT SYSTEM AND THE RESONANCE ELEMENTS.

Receiver Quality Factor ($\mathbf{Q_{RX}}$)	2.6
Resonance frequency ($\mathbf{f_0}$)	65kHz
Coupling Factor(k)	0.40
Load Resistance($\mathbf{R_L}$)	8Ω
Receiver Coil Inductance ($\mathbf{L_{RX}}$)	51μH
Mutual Inductance (M)	41μH
Transmitter Coil Inductance ($\mathbf{L_{TX}}$)	205μH
Receiver Resonance Capacitance ($\mathbf{C_{TX}}$)	115nF
Transmitter Resonance Capacitance ($\mathbf{C_{RX}}$)	29nF

IV. IMPEDANCE MODELLING AND DECOUPLED CONTROL OF THE COMBINED MOTOR AND IPT SYSTEM

Fig. 8 shows the lumped circuit of the combined motor and the IPT system. The converter is modeled as a pulsating voltage source at the switching frequency. The input impedance of the motor and the IPT are shown in Fig. 9.a. Although the motor and IPT have the same switching frequency, the operating frequencies of the DC motor and IPT are far away. V_o has both DC and harmonics of the switching frequency. The switching frequency and IPT resonant frequency are selected compatible, and so the IPT has low-impedance at only the

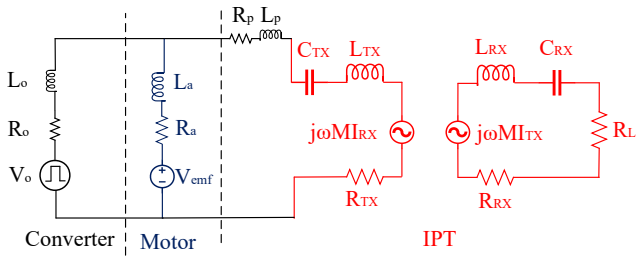

Fig. 8. Combined impedance model of the IPT system and the motor.

switching frequency, which means that IPT filters out DC and other switching harmonics. Besides, the motor is like a low-pass filter, and it filters out the switching harmonics if the motor windings time constant is much longer than the switching period. Thus, the operating frequencies of the motor and IPT system are DC and fundamental switching harmonic, respectively. Then, the motor and the IPT are decoupled considering the difference between their operating frequencies as they behave like high-impedance loads at each other's operating frequency. Moreover, the open and short circuit faults of the IPT are investigated. The open and short circuit conditions are shown in Fig. 9.b, and it is observed that the motor can operate under faults by changing the switching frequency, which ensures high impedance operation of the IPT.

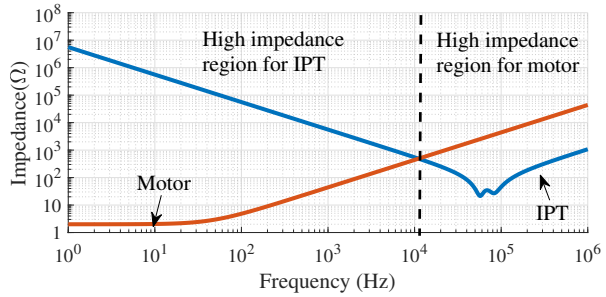

(a) Normal operations of the motor and IPT system.

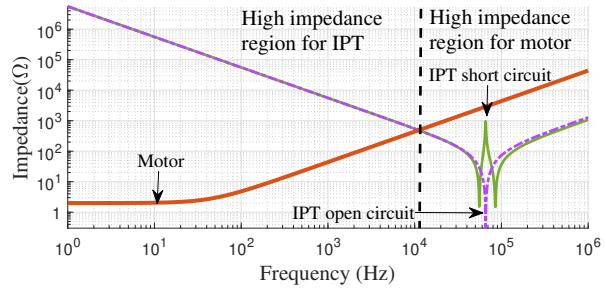

(b) Short and open circuit faults of IPT.

Fig. 9. Frequency response of the motor and the IPT.

As mentioned, operations of the motor and the IPT are decoupled according to the impedance model. However, torque and speed control of the motor and the power control of the IPT system are still challenging. The torque and speed of the motor can be controlled by the duty cycle, and it is independent of the switching frequency. However, the SS-IPT can be controlled by both the duty cycle and the frequency. The variation of the output voltage of SS-IPT (at 80 kHz) with the duty cycle is shown in Fig. 10.a. The variation of the output voltage with the frequency ($D = 0.5$) is shown in Fig. 10.b. Then, the power of IPT is plotted for different duty cycles and frequencies in Fig. 10.c, and it is possible to keep the IPT power constant by moving on the IPT iso-power lines with a proper control of duty cycle and switching frequency.

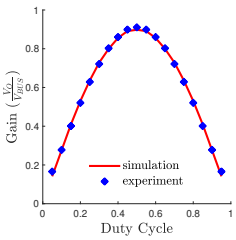

(a)) Duty cycle-gain characteristic of IPT at 80 kHz.

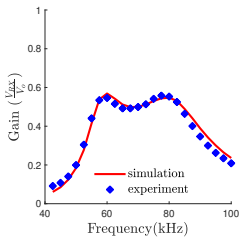

(b) Frequency-gain characteristic of IPT ($D = 0.5$).

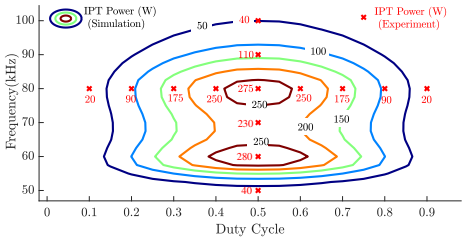

(c) The iso-power lines of IPT through duty cycle and frequency.

Fig. 10. Simulation and experimental results of IPT voltage gain and power as a function of duty cycle and frequency.

The overall control method for the proposed system is given in Fig. 11. The motor controller decides on the duty cycle, which gives the desired speed and torque references. Then, the IPT controller adjusts the switching frequency based on the required output voltage of the IPT system and the duty cycle reference taken from the motor controller.

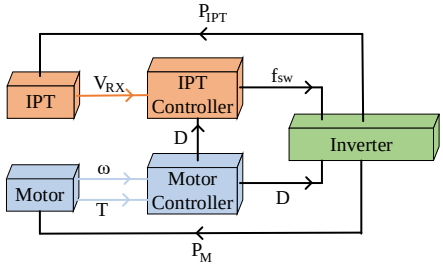

Fig. 11. The block diagram of the control method of the combined motor and IPT system.

V. Experimental Results

In this section, the experimental results using the setup shown in Fig. 6 are presented. Firstly, we will validate the IPT design and compare it with the simulation results. Secondly,

the effect of the IPT system on the motor current is discussed. Thirdly, we will present the results of six different cases to show the feasibility of the proposed system.

A. IPT Tests

TABLE IV
SYSTEM PARAMETERS OF THE SS-IPT

L_{TX}	$205\mu H$
L_{RX}	$51\mu H$
M	$40\mu H$
R_L	8Ω

The IPT system parameters are shown in Table IV. Simulation results, presented in Fig. 10, are repeated with the experimental setup, and the results are compared in Fig. 10. The experimental results have good agreement with simulation results. The difference is around 10% for the operation frequencies between 55 kHz and 100 kHz.

B. Simultaneous operation of the IPT and the motor

Firstly, only the IPT system is connected to the FB converter to operate at 0.85 duty cycle and 81.3 kHz. Fig. 12.a shows the output voltage of IPT (V_{RX}), the output voltage of FB converter (V_o) and the transmitter current (I_{TX}). The V_{RX} and the I_{TX} are 20.8 V_{RMS} and 1.77 A_{RMS}, respectively. Therefore, IPT system transfers 54 W power at this operation point. Then, only the motor is connected to the FB converter, which has the same duty cycle and switching frequency. Fig. 12.b shows the V_o and motor current (I_M). The I_M is 6.85 A, which gives 480 W motor operation. Finally, the motor and IPT system are connected together to the FB converter. The system is operated at the same duty cycle, and switching frequency and Fig. 12.c shows the same voltages and currents. It is observed that the motor currents stay approximately constant with or without the IPT system. In addition, the output voltage of IPT has practically the same with or without the motor. Although these results imply that the IPT and motor operations do not affect each other, the proposed system should also be tested at different operating conditions for verification.

C. Tests under different operating conditions

In this part, the proposed system is examined for six different operating conditions. First, operating points are selected for different power levels of the motor and IPT system. Then, duty cycle and operating frequency are adjusted to provide the required power to the proposed system as summarized in Fig. 11. Table V presents the test parameters for each case. The motor and IPT power are shown in Fig 13. It is shown that the IPT power can be kept constant by frequency control for two different duty cycles, as in cases A and B. In addition, the IPT power can be constant under different motor loads. The transitions of case B to C and E to F show that the IPT powers are the same for two different motor loadings with the same duty cycle and switching frequency. Moreover, the motor power is not affected by the switching frequency

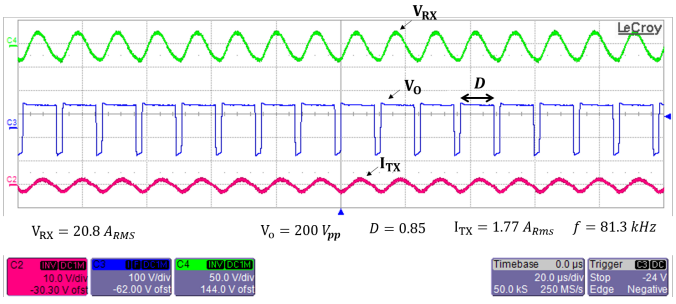

(a) I_{TX},V_{RX} and V_o for only the IPT operation.

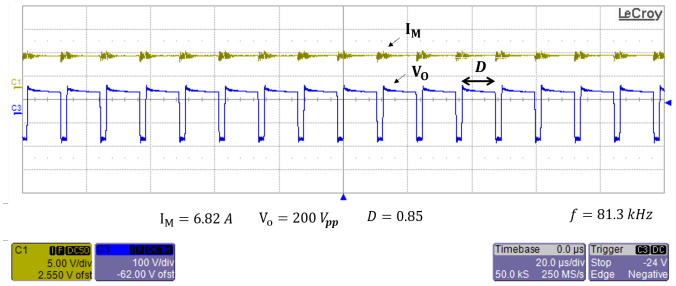

(b) I_M and V_o for only the motor operation.

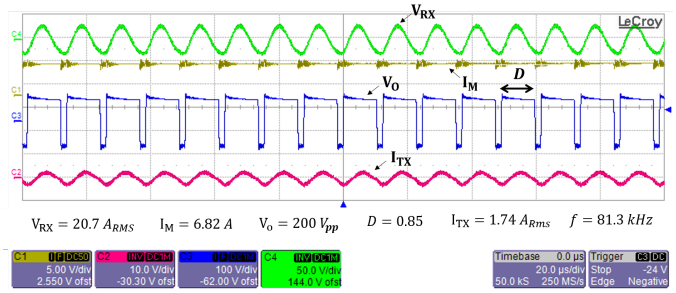

(c) I_{TX},I_M ,$V_{RX}$and V_o for simultaneous the IPT and the motor operations.

Fig. 12. Experiment results for the proposed system with 100 V DC-link.

TABLE V
SIMULTANEOUS OPERATION OF THE IPT AND THE MOTOR UNDER DIFFERENT OPERATING CONDITIONS.

	Cases					
	A	**B**	**C**	**D**	**E**	**F**
Operation Frequency (kHz)	95	90	90	95	90	90
Duty Cycle	0.6	0.75	0.75	0.6	0.6	0.6
Load Torque (N.m)	0.24	0.27	0.37	0.21	0.21	0.17
Motor Power (W)	125	179	244	109	110	89
IPT Power (W)	50	51	51	50	90	90

variations, which is shown by case D to E transition. The previous experiments show that IPT power can be adjusted by frequency and duty cycle control, and the IPT and motor operations are not affected by each other. These test results for different operating conditions conclude that the IPT system and motor can operate for different power ratings, and their operations can be controlled separately by adjusting the duty cycle and switching frequency.

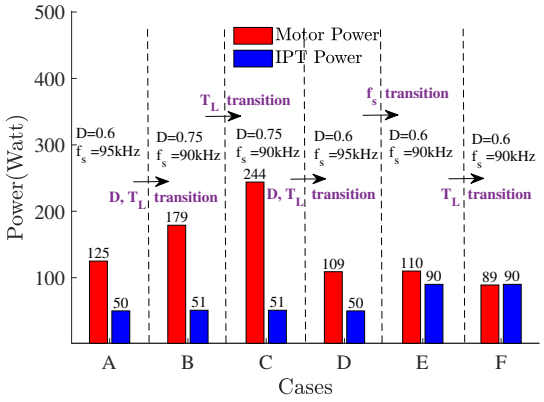

Fig. 13. The power of IPT and motor for cases.

VI. Discussions of the Stress on the DC-Link Capacitor

Unlike a conventional motor driver, the addition of the high-frequency IPT current on the motor driver also increases the stress on the DC-link capacitor. Hence, the system may require a minor modification on the DC-Link capacitance or the type of capacitors. The current, supplied by the DC-link capacitors (I_{CAP}), is expressed as in (7). The S_A and S_B is the switching function of each leg of the converter, as shown in Fig. 3.

$$I_{CAP} = S_A(I_M + I_{TX}) - S_B(I_M + I_{TX}) - I_{in} \quad (7)$$

The motor and IPT currents ($\mathrm{I_M}$ and $\mathrm{I_{TX}}$) are shown in (8). The switching harmonics of the motor current are ignored ($\mathrm{I_{Mdc}}$), and first harmonic approximation (FHA) is applied to the IPT current ($\mathrm{I_{TXf}}$).

$$\begin{aligned} I_M &= I_{Mdc} \\ I_{TX} &= I_{TXf} cos(2\pi f_s t - \Phi) \end{aligned} \quad (8)$$

By using (7) and (8), the DC-link current compenents of the motor and IPT system can be obtained as in (9) and (10) respectively. Therefore, the DC-link current depends on the motor current, duty cycle, and Tx current.

$$I_{capM} = \sum_{k=1}^{\infty} \frac{4I_{Mdc}}{k\pi} sin(k\pi D) cos(2\pi k f_s t) \quad (9)$$

$$\begin{aligned} \mathrm{I_{capTX}} = &- I_{TX} cos(2\pi f_s t - \Phi) \\ &+ \sum_{k=1}^{\infty} \frac{2I_{TX}}{k\pi} sin(k\pi D) cos(2\pi (k+1) f_s t - \Phi) \\ &+ \sum_{k=2}^{\infty} \frac{2I_{TX}}{k\pi} sin(k\pi D) cos(2\pi (k-1) f_s t + \Phi) \end{aligned} \quad (10)$$

Since the capacitor current is affected by both the motor current magnitude and duty cycle, a scenario is created to investigate the capacitor current behavior. In this scenario, the motor current is initially zero at 0.5 duty cycle, and the motor current is linearly increased up to 500W power at 0.85 duty cycle. The DC-link current can be calculated as in (9) when the only motor is connected to the motor driver. The capacitor current for the only motor operation is shown in Fig. 14.a.

Then, the IPT coil is connected parallel to motor windings. The IPT system is desired to supply 50W power for the duty cycle between 0.15 and 0.85. By using (10), the capacitor current, which stems from the IPT system, can also be calculated. In this case, the capacitor current, which consists of both the motor and IPT system, is shown in Fig. 14.b.

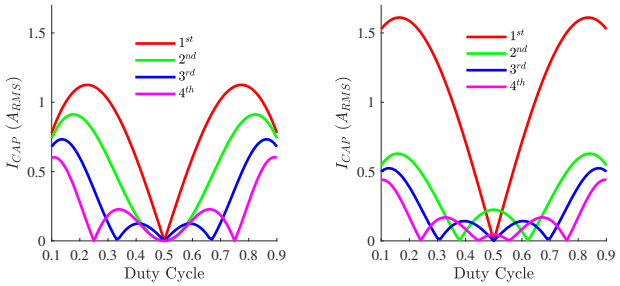

(a) DC-link current, which stems from only the motor.

(b) DC-link current, which stems from the combined motor and IPT system.

Fig. 14. First, second, third and fourth harmonics of the DC link currents as a function of duty cycle.

According to Fig. 14, the motor current that reflects the capacitor current is calculated as 1.45 $\mathrm{A_{RMS}}$, and also the combined motor and IPT system that reflects the capacitor current is calculated as 1.8 $\mathrm{A_{RMS}}$. Hence, the capacitor current is increased by $\%24$ due to the addition of the proposed IPT system. Although the switching frequency does not have a direct effect on the capacitor current stress, the capacitance requirement to minimize voltage ripples is inversely proportional to the switching frequency. Therefore, increasing the switching frequency decreases the capacitance requirement, but the ESR/ESL of the capacitors and parasitic components become more significant at higher frequencies. To sum up, both IPT systems and increasing switching frequency may increase the capacitor current, and voltage stress may result in minor modifications in capacitance or the type of capacitors.

VII. Conclusion

In this article, a novel IPT system to transfer power to rotating systems has been proposed. Unlike conventional systems, the proposed method does not require an extra converter to excite the coils, and the already existing motor driver is utilized to run the motor and transfer power wirelessly. Hence, the complexity and cost are decreased, which increases the feasibility of such a system. However, the selection of switching frequency is challenging since a high switching frequency increases the converter losses, and a low switching frequency increases the IPT coil size and cost. With the development of wide band-gap devices such as GaN, there could be found a sweet spot, satisfying both requirements. Therefore, a combined IPT system and motor driver with a single converter can be established using a GaN based voltage source converter. DC-link capacitor stress due to the extra IPT system is investigated in this study, and it is concluded

that the IPT system can be implemented to any conventional motor driver with maybe a slight modification to the DC-link capacitors. The proposed system has been tested via an experiment setup, which provides operation at 500 W motor power and 50 W IPT power. Besides, various operation cases were presented, and the transition of the operations was discussed regarding the change in frequency, duty cycle, and load torque. It was observed that the motor and IPT systems could be operated in different conditions. The proposed system can be utilized for any auxiliary loads in another system since it can be expanded and generalized for other industrial motors, such as single-phase or multi-phase AC motors.

REFERENCES

[1] M. Maier and N. Parspour, "Operation of an electrical excited synchronous machine by contactless energy transfer to the rotor," *IEEE Transactions on Industry Applications*, vol. 54, no. 4, pp. 3217–3225, 2018.

[2] K. Song, B. Ma, G. Yang, J. Jiang, R. Wei, H. Zhang, and C. Zhu, "A rotation-lightweight wireless power transfer system for solar wing driving," *IEEE Transactions on Power Electronics*, vol. 34, no. 9, pp. 8816–8830, 2019.

[3] G. He, Q. Chen, X. Ren, S. Wong, and Z. Zhang, "Modeling and design of contactless sliprings for rotary applications," *IEEE Transactions on Industrial Electronics*, vol. 66, no. 5, pp. 4130–4140, 2019.

[4] M. R. Barzegaran, H. Zargarzadeh, and O. A. Mohammed, "Wireless power transfer for electric vehicle using an adaptive robot," *IEEE Transactions on Magnetics*, vol. 53, no. 6, pp. 1–4, 2017.

[5] H. Polat, "Fault tolerant modular inductive power transfer system design using resonator coil," Apr 2021. [Online]. Available: https://www.techrxiv.org/articles/preprint/Fault_Tolerant_Modular_Inductive_Power_Transfer_System_Design_Using_Resonator_Coil/14370617/1

[6] Y. H. Sohn, B. H. Choi, E. S. Lee, G. C. Lim, G. Cho, and C. T. Rim, "General unified analyses of two-capacitor inductive power transfer systems: Equivalence of current-source ss and sp compensations," *IEEE Transactions on Power Electronics*, vol. 30, no. 11, pp. 6030–6045, 2015.

[7] J. Zeng, G. Zhang, S. S. Yu, B. Zhang, and Y. Zhang, "Llc resonant converter topologies and industrial applications — a review," *Chinese Journal of Electrical Engineering*, vol. 6, no. 3, pp. 73–84, 2020.

[8] X. Qu, H. Chu, S. Wong, and C. K. Tse, "An ipt battery charger with near unity power factor and load-independent constant output combating design constraints of input voltage and transformer parameters," *IEEE Transactions on Power Electronics*, vol. 34, no. 8, pp. 7719–7727, 2019.

[15] J. Dai, S. Hagen, D. C. Ludois, and I. P. Brown, "Synchronous generator brushless field excitation and voltage regulation via capacitive coupling through journal bearings," *IEEE Transactions on Industry Applications*, vol. 53, no. 4, pp. 3317–3326, 2017.

[9] S. Tiwari, O. . Midtgård, and T. M. Undeland, "Sic mosfets for future motor drive applications," in *2016 18th European Conference on Power Electronics and Applications (EPE'16 ECCE Europe)*, 2016, pp. 1–10.

[10] V. Shevchenko, O. Husev, R. Strzelecki, B. Pakhaliuk, N. Poliakov, and N. Strzelecka, "Compensation topologies in ipt systems: Standards, requirements, classification, analysis, comparison and application," *IEEE Access*, vol. 7, pp. 120 559–120 580, 2019.

[11] A. K. Morya, M. C. Gardner, B. Anvari, L. Liu, A. G. Yepes, J. Doval-Gandoy, and H. A. Toliyat, "Wide bandgap devices in ac electric drives: Opportunities and challenges," *IEEE Transactions on Transportation Electrification*, vol. 5, no. 1, pp. 3–20, 2019.

[12] W. Lee, S. Li, D. Han, B. Sarlioglu, T. A. Minav, and M. Pietola, "A review of integrated motor drive and wide-bandgap power electronics for high-performance electro-hydrostatic actuators," *IEEE Transactions on Transportation Electrification*, vol. 4, no. 3, pp. 684–693, 2018.

[13] E. A. Jones, F. F. Wang, and D. Costinett, "Review of commercial gan power devices and gan-based converter design challenges," *IEEE Journal of Emerging and Selected Topics in Power Electronics*, vol. 4, no. 3, pp. 707–719, 2016.

[14] D. C. Ludois, J. K. Reed, and K. Hanson, "Capacitive power transfer for rotor field current in synchronous machines," *IEEE Transactions on Power Electronics*, vol. 27, no. 11, pp. 4638–4645, 2012.

[16] H. Hu, T. Cai, S. Duan, X. Zhang, J. Niu, and H. Feng, "An optimal variable frequency phase shift control strategy for zvs operation within wide power range in ipt systems," *IEEE Transactions on Power Electronics*, vol. 35, no. 5, pp. 5517–5530, 2020.

[17] M. Kumar, R. K. Yakala, S. Pramanick, and B. K. Panigrahi, "Improved interconnect layout of dc link capacitor bank to minimize parasitic inductance and its effect on performance of sic mosfet," in *2020 IEEE International Conference on Power Electronics, Smart Grid and Renewable Energy (PESGRE2020)*, 2020, pp. 1–6.

[18] A. Safaee and K. Woronowicz, "Time-domain analysis of voltage-driven series–series compensated inductive power transfer topology," *IEEE Transactions on Power Electronics*, vol. 32, no. 7, pp. 4981–5003, 2017.

[19] Y. Fang and B. M. H. Pong, "Multiple harmonics analysis for variable frequency asymmetrical pulsewidth-modulated wireless power transfer systems," *IEEE Transactions on Industrial Electronics*, vol. 66, no. 5, pp. 4023–4030, 2019.

[20] F. Karakaya, O. S. Alemdar, and O. Keysan, "Layout Based Ultra-Fast Short-Circuit Protection Technique for Parallel Connected GaN HEMTs," *IEEE Journal of Emerging and Selected Topics in Power Electronics*, pp. 1–1, 2021.

[21] K. Aditya and S. S. Williamson, "Design guidelines to avoid bifurcation in a series–series compensated inductive power transfer system," *IEEE Transactions on Industrial Electronics*, vol. 66, no. 5, pp. 3973–3982, 2019.